IET Microwaves, Antennas & Propagation

Research Article

IET Journals
The Institution of Engineering and Technology

Wideband stripline fed tapered slot antenna with integral coupler for wide scan angle active phased array

ISSN 1751-8725
Received on 17th August 2017
Revised 31st January 2018
Accepted on 2nd March 2018
doi: 10.1049/iet-map.2017.0784
www.ietdl.org

Priya Suresh Nalumakkal[1] ✉, K. Maheshwara Reddy[1], K.J. Vinoy[2], Saurabh Shukla[1]

[1]*DRDO, Defence Avionics Research Establishment, Bangalore, India*

[2]*Department of Electrical Communication Engineering, Indian Institute of Science, Bangalore, India*

✉ *E-mail: priyasuresh298@gmail.com*

Abstract: A stripline fed tapered slot antenna (STSA) with integral coupler operating as an active array element over 1.5 octave bandwidth is presented. The proposed STSA with integral coupler features wideband transition which allows a direct 50 Ω stripline feed and enables the coupler to be integrated along with the feed. The coupler helps in taking a sample of signal for online performance monitoring and active phased array calibration. The measured results of antenna element have exhibited good radiation pattern performance with low cross-polarisation in principal plane and low beam squint. Using this, a 16-element *H*-plane linear phased array antenna designed for the frequency range of 6–18 GHz and azimuth scan coverage of 60° is also presented. The active reflection coefficient of the array is calculated from measured mutual coupling coefficients and the array pattern over different scan angles is demonstrated. The grating lobe free scan coverage of 60° is obtained. The antenna array finds application in airborne systems.

1 Introduction

Modern-day multi-functional applications for radar, communications and electronic warfare utilise active phased array (APA) as radiating apertures. These have high effective radiated power and thus high detection ranges [1]. Electronic warfare applications require phased array antennas in electronic counter measure (ECM) with wide bandwidth, high beam agility, high pointing accuracy and wide scan angle capabilities [2]. Antenna element for a wideband phased array for the above-mentioned applications should possess a wide bandwidth and an appropriate beamwidth to get the required scanning performance and a compact size to allow for a sufficiently small array lattice that prevents grating lobe formation at the maximum operating frequency. When the same ECM phased array is used for direction finding, the additional desirable features are low or zero beam squint and low cross-polarisation in the principal plane [3, 4]. A stripline fed tapered slot antenna (STSA) is a promising candidate for this application since it has been shown to exhibit the desired characteristics of wide bandwidth, wide beamwidth for scanning and low cross-polarisation [5, 6]. A recent work on stripline fed bilateral tapered slot antenna (TSA) [7] has exhibited a wide bandwidth and cross-polarisation of −25 dB.

For the proper functioning of a phased array it is essential to have performance monitoring (PM) and online calibration [8]. The array is calibrated to obtain a coherent beam with maximum gain by measuring the output signal at all antenna elements, relative to each other with respect to a known input signal. One of the approaches for the wideband phased array is to tap a signal through a power divider or a directional coupler at the input of each of antenna element [8, 9]. Hence in wideband phased arrays, it is required to have a provision to integrate a directional coupler along with the feed line of each element. A substrate integrated waveguide coupler for antipodal TSAs for adaptive receiver application is reported in [10]. This operates for less than an octave bandwidth. However, for multi-octave applications a stripline coupler integral to STSA is the obvious and a novel choice.

A STSA reported in [7] has a wideband transition with low input impedance. This antenna can be fed directly by a 50 Ω stripline, without impedance transformers. This feeding mechanism is adopted to implement a multi-octave bandwidth stripline coupler integral to the feed of the STSA.

Another variant of TSA, a double exponentially TSA working over 1.77 octave bandwidth reported in [11] also has low input impedance and is fed directly by a 50 Ω SMA connector. The electrical dimensions of the antenna at low frequency are $1.4\lambda_0$ length and $0.686\lambda_0$ width. The thickness is 200 μm. Due to the thin profile and flexible nature it is more suitable as a conformal antenna than as an array element.

In this paper, we report the design and experimental validation of an STSA with integral coupler (Fig. 1) as an active array antenna element and a 16-element linear array that operates over 6–18 GHz bandwidth. Section 2 presents the selection and design of antenna element and coupler. Section 3 presents the antenna fabrication and results. Section 4 discusses the performance of the element in the array environment. Section 5 presents the 16-element array configuration, characterisation and results. Section 6 provides conclusions of this work.

2 Antenna geometry

2.1 Design requirements

The objective is to design an antenna element for a linear APA antenna that operates over 6–18 GHz with a minimum array gain of 12 dB at boresight and scan coverage of ± 60° in *H*-plane (Az). Specifications of this element are discussed in Table 1. In order to avoid grating lobes within scan coverage of θ_0, the inter-element spacing (IES) of the array is given by [1]

$$\text{IES} < \lambda_{\text{hi}}/(1 + \sin(\theta_0)) \tag{1}$$

where λ_{hi} is the wavelength at the highest frequency. Hence for 60° scan this limit comes to $0.535\lambda_{\text{hi}}$ (8.9 mm), which also limits the class of radiating elements used for this application.

TSAs are one of the classes of endfire antennas suitable for this application. Several TSA types exist, the most common being linear tapered (LTSA), exponential tapered (Vivaldi) and constant width (CWSA). The previous studies emphasised the dependence of beamwidth, gain and side lobe level on taper profile [12]. For a given length and width, the exponential TSA provides largest beamwidth and lowest side lobe level followed by LTSA and CWSA. In addition to these, the exponential TSA provides a low cross-polarisation in *H*-plane [13]. Since the requirement is for a

© The Institution of Engineering and Technology 2018

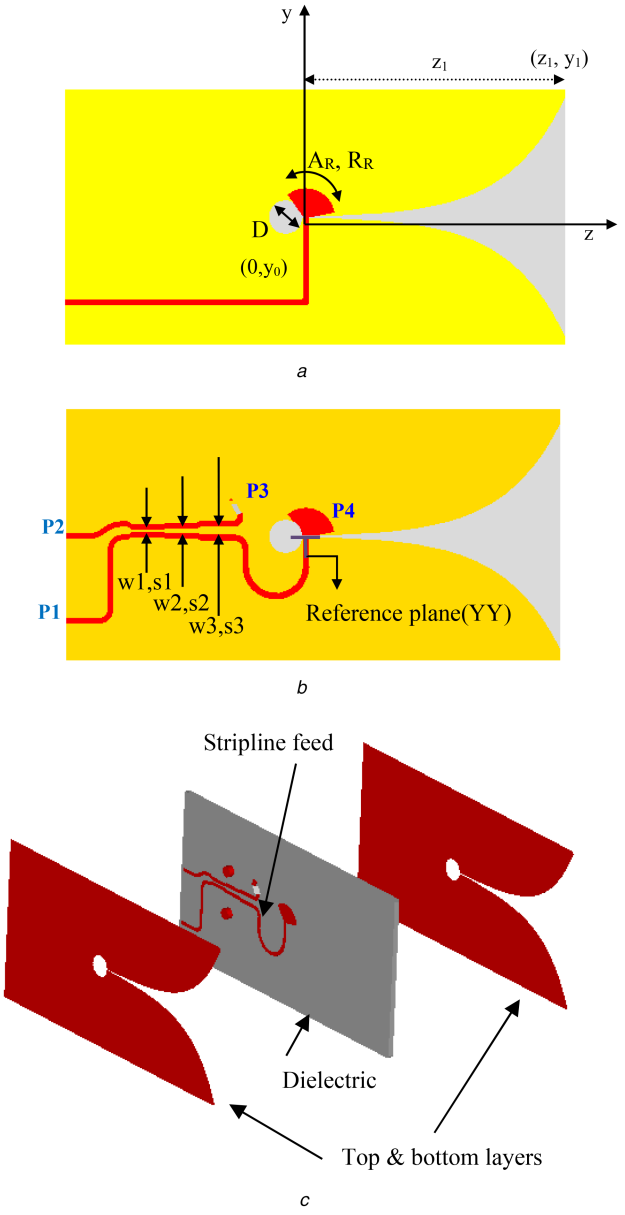

Fig. 1 *Geometry and configuration of STSA*

(a) Description of geometry and definition of parameters, ***(b)*** Configuration of proposed STSA with integral coupler showing all the ports, ***(c)*** Exploded view showing the three layers

wider beamwidth in *H*-plane and low cross-polarisation, an exponential TSA is the obvious choice.

The exponential TSA generally may consist of either planar or antipodal geometry [14]. A planar TSA, in general, may be fed by a microstrip or a strip line. One of the serious drawbacks of microstrip-fed planar TSA is the difficulty in the impedance matching of the slotline at the input of the antenna. Slotlines fabricated on a low dielectric constant substrate have high impedance, which makes the matching to a 50 Ω feed difficult [15, 16]. The same issue persists with stripline fed planar TSA such as the one reported in [17]. This can be overcome partially by using antipodal geometry. Antipodal antennas are wideband in nature [18] but often has a cross-polarisation of −15 dB at 18 GHz [19]. Another problem reported for such antennas is the beam squint in the *E*-plane beam. A squint of 15° is reported in [19] and is brought down to 4° by a technique of substrate end shaping [20].

An STSA is superior with respect to its low cross-polarisation in principal plane, low beam squint and can facilitate an integral coupler along with the feed [7]. Therefore in the present work, an STSA whose geometry is given in Fig. 1 is selected as a suitable candidate and proposed as the array element.

Table 1 Key specifications of the proposed antenna element for the linear APA antenna

Parameter	Value
frequency range	6–18 GHz
reflection coefficient over frequency	better than −10 dB
gain over frequency 3 dB beamwidth in array environment	moderate gain of 4–10 dB 120° in *H*-plane, 60° in *E*-plane
cross-polarisation in the principal plane	better than −25 dB at boresight
beam squint	<1°

Table 2 Final optimal dimensions of the TSA shown in Fig. 1 (unit: mm)

Dimension	Value
y_1	30
y_0	30
z_1	15
R_R (radius of radial stripline stub)	3.4
A_R (angle of radial stub)	114°
D (diameter of circular cavity)	4
w_1 (width of stage 1 of coupler)	0.66
s_1 (spacing of stage 1 of coupler)	0.25
w_2 (width of stage 2 of coupler)	0.71
s_2 (spacing of stage 2 of coupler)	0.55
w_3 (width of stage 3 of coupler)	0.74
s_3 (spacing of stage 3 of coupler)	0.9

E-plane of the antenna is *zy*-plane and *H*-plane is *zx*-plane. It has three conducting layers, top and bottom with radiating slots also known as bilateral slot (identical slots in both ground planes of stripline), fed by stripline in the middle layer, which is etched on one side of bottom substrate.

Assuming antenna is placed in *yz*-plane and the axis is aligned along *z*-direction, the flare of the antenna is described by the exponential taper

$$y = y_0 + \frac{(y_1 - y_0)\,(e^{\alpha z} - 1)}{(e^{\alpha z_1} - 1)} \tag{2}$$

where the taper factor chosen is $\alpha = 0.15$. $(y_0, 0)$ and (y_1, z_1) are coordinates of initial and final points of taper as in Fig. 1*a*. The design of TSA is primarily based on empirical approach [14]. The width of TSA should be at least $\lambda_0/2$ for efficient radiation, where λ_0 is the free space wavelength at the lowest frequency and hence is chosen as $0.6\lambda_0$. The antenna geometry is fine-adjusted to satisfy the requirement of broad beamwidth in azimuth and moderate gain with return loss better than 10 dB by full-wave simulations using CST Microwave Studio [21]. The final dimensions of the antenna are given in Table 2.

2.2 Design of antenna feed

In this work, we use stripline to feed the planar bilateral slotline input of the antenna. Input impedance of 50 Ω is achieved by choosing substrate Rogers RT Duroid 5870 ($\varepsilon_r = 2.33$) with thickness 40 mil (by lamination of two 20 mil substrates) and slot width at antenna input as 0.2 mm. As a result, it can be fed directly from 50 Ω stripline without impedance matching transformers.

Impedance bandwidth of 3:1 is achieved in this design by using a radial stub and circular cavity, which acts as virtual short and open, respectively [15]. The optimal dimensions of the feed structure obtained by simulations are given in Table 2. The impedance characteristics of the antenna with feed are extracted using the equivalent circuit [22] as referred in the inset of Fig. 2.

© The Institution of Engineering and Technology 2018

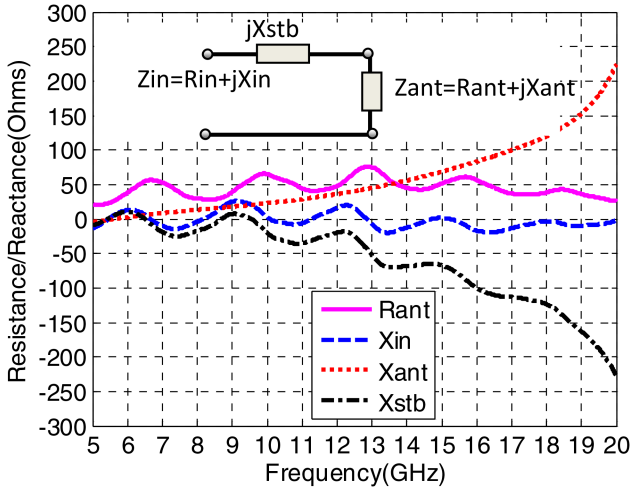

Fig. 2 *Design of the wideband matching of STSA. The equivalent circuit of antenna with feed is shown in the inset*

The total impedance Z_{in} at the reference plane *YY* (as marked in Fig. 1*b* at the junction of the stripline feed and the slotline) is expressed as series connection of the stripline stub reactance jX_{stb} and the antenna impedance $Z_{ant.}$. The Z_{in} and jX_{stb} are obtained by simulations by separately analysing the input impedance of the full antenna structure and reactance of stripline radial stub (without bilateral slotline of antenna) at the reference plane using 'de-embed *S*-parameter' under *S*-parameter calculation in CST. It is observed from Fig. 2 that the reactance of antenna with cavity is cancelled by the reactance of radial stub.

Reactance part of total impedance at the reference plane fluctuates around zero. It may also be noted that the resistance part of impedance at reference plane is close to 50 Ω, which makes it a simple feed.

2.3 Design of the integral coupler

In this work, a −22 dB directional coupler integral to the stripline feed of the STSA is used for PM and calibration of individual elements of an array. This coupling level is suitable for signal injection without disturbing the array performance. Due to weaker coupling requirement, an edge coupled coupler is preferred for easy fabrication [23].

Due to large bandwidth of the antenna, the coupler must have wide bandwidth with small ripple, small size and low insertion loss. Hence, an asymmetrical edge coupler is designed [24]. Stripline is preferred medium for a multi-section coupler to ensure equal even and odd mode phase velocities [25]. The width and gap of coupler are computed from the even and odd mode impedance provided in Levy's table [26].

The coupler integral to antenna is modelled and simulated using CST. The width and gap of each section obtained after fine adjustment is included in Table 1. Each section of the coupler is 4.08 mm in length. Referring to Fig. 1*b*, P1 is the input port, P2 is the coupled port, P3 is the isolated port and P4 is the through port.

The isolated port P3 is terminated internally with a resistor realised using Ohmega Ply resistive layer [27], where it sees a resistive termination for perfect matching condition and the through port P4 is terminated by the radial stub. The coupler port is routed in the centre of the antenna element to make the mechanical interface easy.

3 Antenna element fabrication and results

Fig. 3*a* shows the photograph of the fabricated antenna based on the dimensions in Table 2. This is fabricated by lamination of two 20 mil RT Duroid 5870 substrates glued with the help of Prepreg 3001. Due to larger number of radiating elements, simple press-on connections are desirable and used for each ports. The coupler port is fed by Gilbert make GPO connector and antenna port through Tyco make BMA connector. A mechanical interface is used to pack

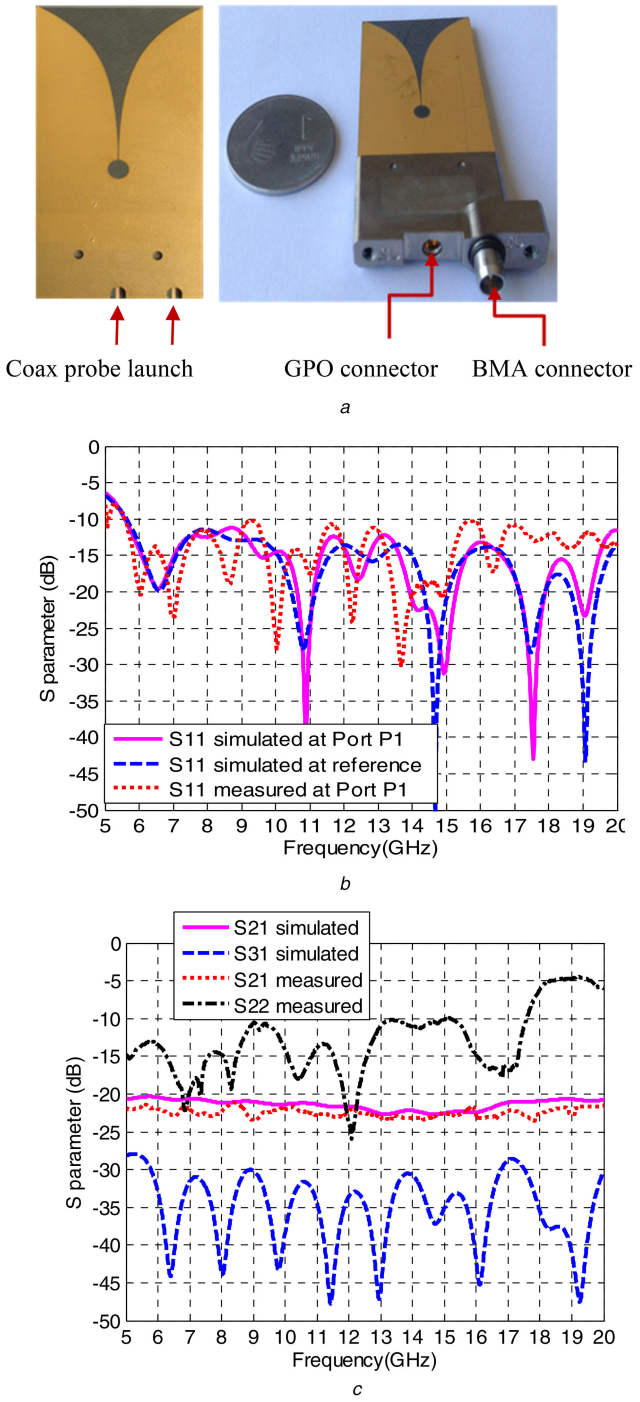

Fig. 3 *Fabricated STSA with results*

(a) Photograph of STSA with different connectors used and close-up view, ***(b)*** Simulated and measured S_{11} at the antenna port compared with the simulated S_{11} without the coupler (at the reference plane), ***(c)*** *S*-parameters of coupler integral to antenna

the stripline feed and coupler and to hold STSA as cantilever, as well as GPO and BMA connectors. BMA connector probe is launched directly on the stripline through a cut provided on the top layer of the antenna as shown in Fig. 3*a*.

3.1 Results of antenna element and the integral coupler

STSA is characterised for its reflection coefficient performance using a vector network analyser (VNA). The simulated reflection coefficient at the reference plane *YY* and the antenna port P1 are plotted in Fig. 3*b*. The two results closely follow and hence it may be concluded that the introduction of coupler has not deteriorated the antenna reflection coefficient. The measured reflection

© The Institution of Engineering and Technology 2018

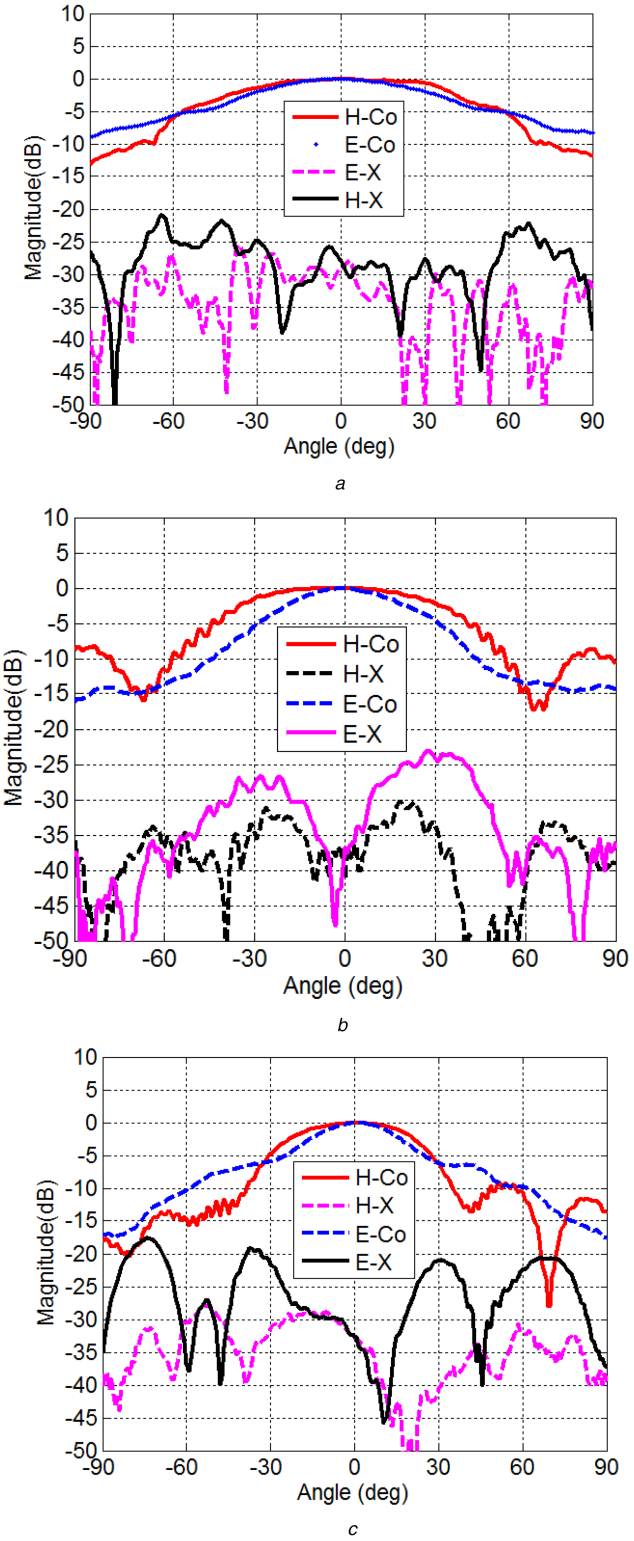

Fig. 4 *Measured H- and E-plane radiation patterns of single element at* ***(a)*** 6 GHz, ***(b)*** 12 GHz, ***(c)*** 18 GHz

coefficient at port P1 is presented in Fig. 3*b* and is better than −10 dB over 6–18 GHz.

The simulated and measured *S*-parameters of coupler integral to antenna are plotted in Fig. 3*c*. The measured data is of coupler integral to antenna and not a separate fabricated piece with four ports.

A reflection coefficient of better than −10 dB is observed in the majority of bands and a maximum value of −6 dB is observed at 18 GHz. The increase in return loss is due to the termination of isolated port internally, which has frequency dependence due to the parasitic effects [28]. This is a limitation or maximum achievable results, due to the space constraints to accommodate a broadband

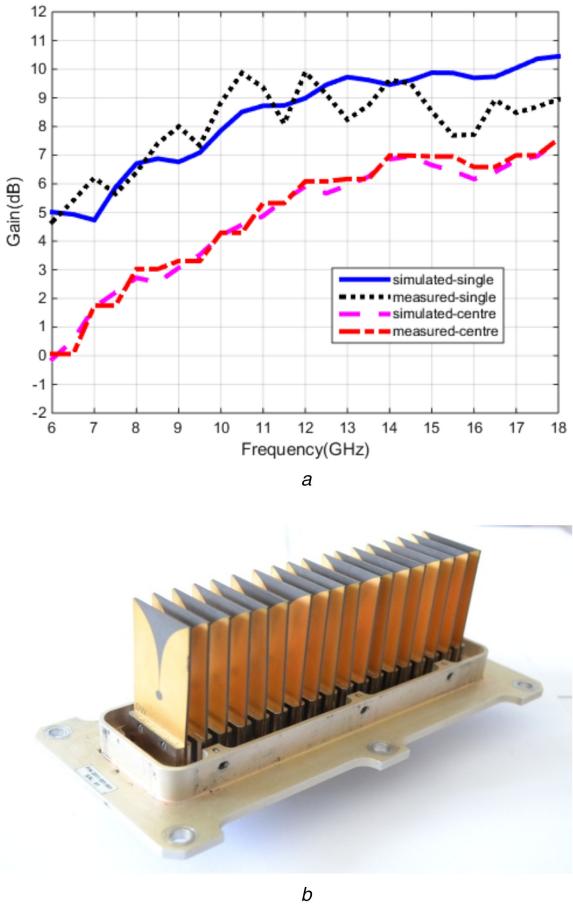

Fig. 5 *Fabricated array with Gain plots*

(a) Simulated and measured gain of isolated single element and the gain of centre element in array, ***(b)*** Photograph of the fabricated 16-element linear array

matching circuit. The coupler output of −22 dB with ripple better than ± 1.5 dB is achieved over the frequency band. The increase in ripple may be due to the poor return loss of the coupled port P2 and also due to the wide variation in load R_{ant} at port P4 as referred in Fig. 2.

From a system point of view, the increase in ripple over frequency is of no concern since the coupler O/P is used for calibration whereas the ripple across channels is rather important.

Since port P3 of the coupler is resistively terminated internally, the isolation of the coupler (S_{31}) is presented only as results of EM simulation. The worst case isolation observed is 28 dB. Other parameters such as reflection coefficient at the coupled port (S_{22}) and coupler output (S_{21}) are presented with measured results for the realised antenna. The measured S_{21} is compared with simulated results in Fig. 3*c*.

The radiation patterns in the *E*- and *H*-planes along with their respective cross-polar plots at 6, 12 and 18 GHz have been measured in an indoor far-field anechoic chamber and presented in Fig. 4.

The *H*-plane beamwidths at the three frequencies are 90°, 70° and 50°, respectively, and *E*-plane are 70°, 60° and 45°, respectively. Cross-polarisation levels of the antenna element are presented and are better than −30 dB at 18 GHz for both *E*-and *H*-planes. There is no beam squint observed for the *H*-plane patterns and a squint of <1° is observed for the *E*-plane patterns. Simulated and measured boresight gain of the single element is presented in Fig. 5*a*. The measured gain varies from 4.6 to 10 dB.

© The Institution of Engineering and Technology 2018

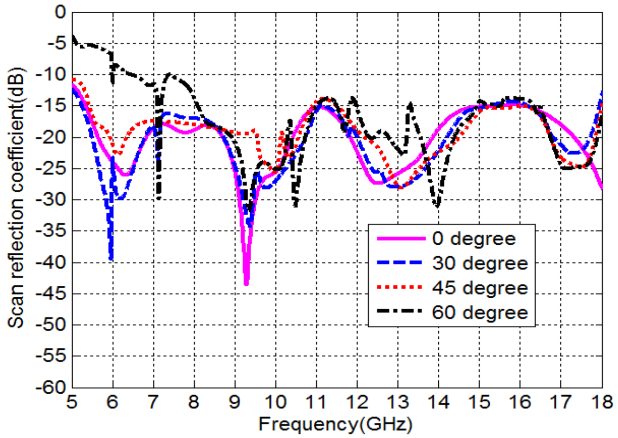

Fig. 6 *Simulated scan reflection coefficient (for infinite array) at broadside (0° scan) as well as for different scan angle at an IES of 0.516λ_{hi} at 18 GHz*

4 Performance of the element in array environment

4.1 Scan reflection coefficient

Performance of the element in array environment is predicted by determining the scan reflection coefficient at different scan angles for an infinite array. Elements in an active array have a scan reflection coefficient or active reflection coefficient [29], defined as the reflection seen at the input of the antenna elements when all elements are transmitting (active). The infinite array simulations are done by setting appropriate boundary conditions: a periodic boundary in *H*-plane and open boundary in other planes. Referred to Section 2, the IES must not exceed 0.535λ_{hi} (8.9 mm). In addition, grating lobe theory suggests that scan performance is improved by reducing the element spacing as small as possible [6]. Hence, simulations are done for two different spacing of 0.529λ_{hi} (8.8 mm) and 0.49λ_{hi} (8.2 mm) at 18 GHz. From the results with spacing of 0.529λ_{hi}, it is observed that there is a peak in the scan reflection coefficient for all scan angles at 17.9 GHz. This is most likely caused by the first grating lobe. For the spacing of 0.49λ_{hi}, the scan reflection coefficient is poor for 60° scan at the lower end of frequency band. Hence, an optimum value of 0.516λ_{hi} (8.6 mm) is chosen. The results of scan reflection coefficient for scan angles 0°, 30° and 45° over the band are given in Fig. 6 and are better than −10 dB, whereas for 60° scan, it is better than −10 dB over the band except for a small deviation around 6–6.4 GHz. Here it goes to a maximum of −8.4 dB. However, there would be a deviation on the results at low frequencies due to truncation effects of the finite array [30].

5 16-element linear array configuration, fabrication and results

5.1 Configuration of the array

The IES is set at 0.516λ_{hi} (8.6 mm). The number of elements is derived from the requirement of array gain. The expression for array gain is given as [1, 8]

$$G = G_e(\theta)\, x\, G_a(\theta)\,. \tag{3}$$

where G_e is the element factor, $G_a = 10{*}\log(N)$ is the array factor consisting of N array of isotropic elements.

The element factor of the array is the gain of the centre element in array environment. The simulated centre element gain is presented in Fig. 5*a*. It is observed that a 0 dB gain is obtained at 6 GHz. Due to mutual coupling effect there is a reduction in gain compared to isolated single element. Hence, to achieve an array gain of 12 dB at boresight, a 16-element array is configured.

The array is fabricated based on the optimised IES of 0.516λ_{hi} (8.6 mm). Fig. 5*b* shows the photograph of the fabricated array. The array is characterised to obtain the average active element gain pattern, mutual coupling coefficients and the pattern performances.

5.2 Measured average active element gain pattern

The overall array performance is expressed as the product of isotropic array factor and scan element pattern. The array radiation pattern for an N-element linear phased array is expressed as [31]

$$S(\theta) = S_e(\theta) \sum_{i=1}^{N} a_i e^{-j[k(N-i)dx\sin(\theta)+\Psi i]} \tag{4}$$

where S_e (θ) is the scan element pattern, a_i is the amplitude distribution, k_0 is the free space wave number, dx is the IES between elements and $\Psi i = -k_0(N-i)dx\sin(\theta_0)$.

The scan element pattern shows array gain versus scan angle and is a useful performance measure from a system point of view. Conventionally, the centre element pattern is used to represent the scan element pattern for a large phased array. For small wideband arrays the edge effects become prominent at lower frequency [6, 30] and hence the mutual coupling affects the radiation of each element differently. Hence, an average active element gain pattern, which is calculated by measuring and averaging the entire elements pattern in array structure, is used to represent the element factor of the array [32].

Hence, the present 16-element linear array is characterised using the average active gain pattern. Here the mutual coupling of the array is exploited to improve the beamwidth and hence more angular coverage and thus more scan angle coverage.

Measured average active gain pattern of the array in *H*-plane and *E*-plane are shown in Fig. 7. Here the average active gain patterns exhibit an increase in the beamwidth and decrease in gain in the array environment than the single element pattern. The −3 dB beamwidth obtained are 130°, 120° and 100° in *H*-plane and there is not much variation in *E*-plane as compared to single element. Reduction in beamwidth at higher frequencies is compensated by the increase in gain to achieve the required scan angle of ± 60°.

5.3 Measured mutual coupling

The mutual coupling at all the elements of the 16-element linear array with the centre element excited are measured as *S* parameters using VNA and shown in Fig. 8. While carrying out the measurements, all elements other than the centre element and the element where measurement is to be taken are terminated with 50 Ω. The maximum coupling of −12 dB at 8.5 GHz is observed for the centre element to the neighbouring elements.

The active reflection coefficient is computed from the measured mutual coupling coefficients. For a uniformly fed N element linear array pointing at θ_0 the scan reflection coefficient of mth element is defined as [31, 33]

$$\Gamma_m(\theta_0) = \sum_{n=1}^{N} S_{mn} e^{-jkndx\sin\theta_0} \tag{5}$$

© The Institution of Engineering and Technology 2018

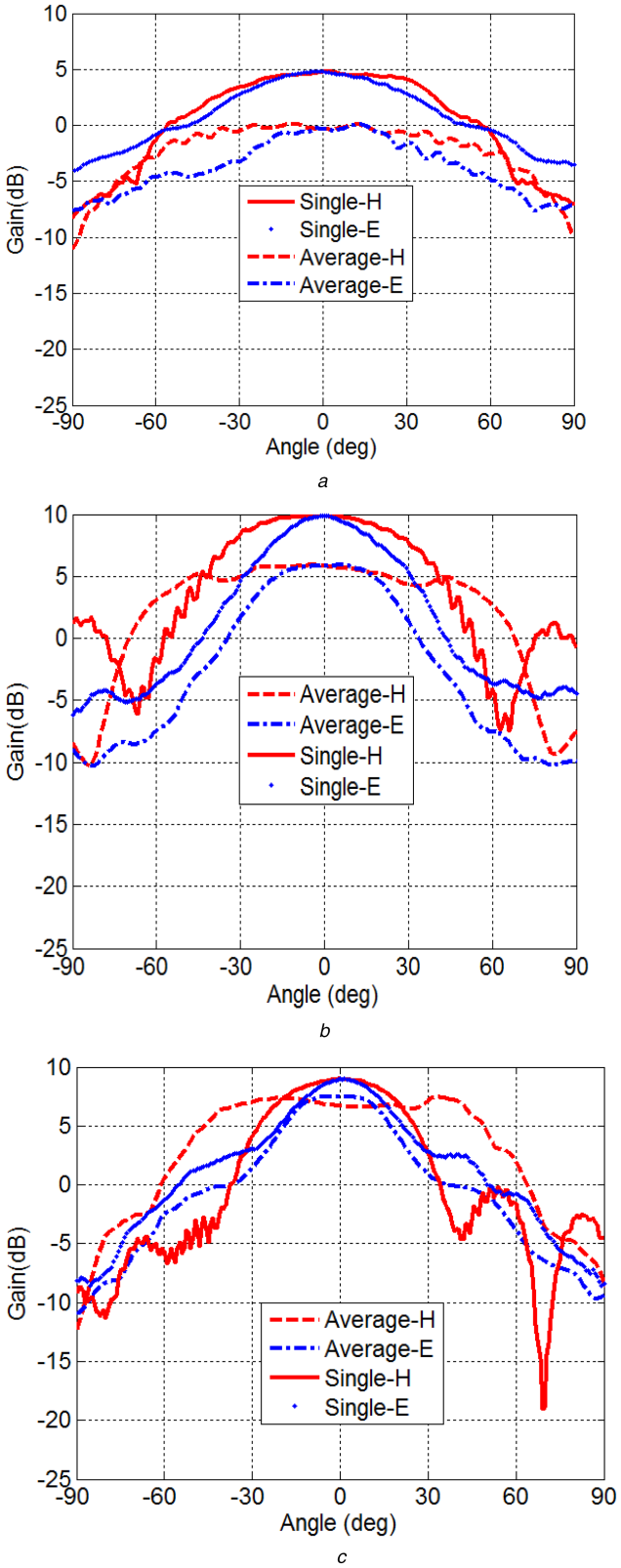

Fig. 7 *Measured H- and E-plane radiation patterns of single element and the average active gain pattern of the 16-element linear array at* ***(a)*** 6 GHz, ***(b)*** 12 GHz, ***(c)*** 18 GHz

In (2), S_{mn} is the measured coupling coefficients, k is the free space wave number, dx is the linear spacing between elements. The computed active reflection coefficient at broadside of centre element of the 16-element linear array is presented in Fig. 8. It is reasonable to assume that the peaks at low frequencies are due to edge reflections.

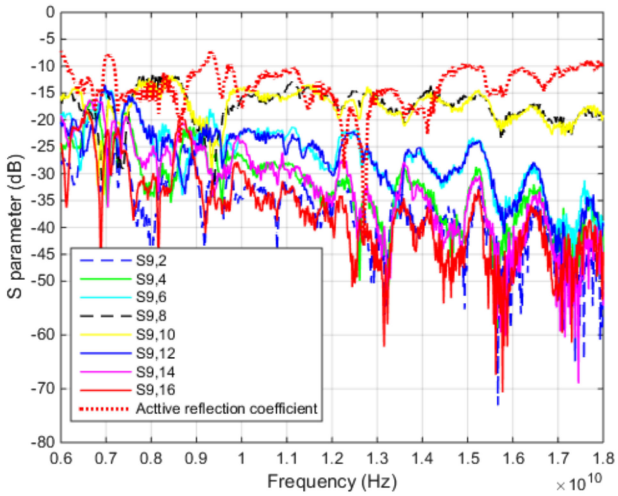

Fig. 8 *Measured mutual coupling between the centre element and the even numbered elements and the computed active reflection coefficient of the centre element*

5.4 Measured active array pattern

The scan performance of array is also done by steering the beam. All the elements are excited by giving uniform amplitude and the phase is varied. Phase control is done by using a commercially off the shelf monolithic microwave integrated circuit-based digital phase shifter module. The characterisation is done in an indoor far-field anechoic chamber in receive mode of the array. The array pattern obtained for 6, 12 and 18 GHz for broadside, 30° and 60° scan angles is presented in Fig. 9. It is observed that there is no grating lobe within the scan coverage. The beamwidths obtained are 18.75° at 6 GHz, 9.53° at 12 GHz and 6.35° at 18 GHz. The results of cross-polarisation at boresight are 43 dB at 6 GHz, 40 dB at 12 GHz and 30 dB at 18 GHz. During the scan, the beamwidth broadens approximately inversely to the cosine of the scan angle [1, 31]. The maximum side lobe levels observed at broadside are 13, 11.69 and 10.49 dB at 6, 12 and 18 GHz, respectively. The deviation from the theoretical maximum of −13.15 dB is due to the phase quantisation error of digital phase shifter. This can be improved by using a higher bit phase shifter.

6 Conclusions

The design and development of a STSA with integral coupler for wide scan angle *H*-plane linear phased array antenna operating over a frequency band of 6–18 GHz is presented. The measured results of STSA have shown a reflection coefficient better than −10 dB, a moderate gain of 4.6–10 dB and a broad beamwidth. Very good radiation pattern characteristics are demonstrated with cross-polarisation of better than −30 dB and beam squint <1°.

The tri-section stripline coupler is designed along the feed line of the antenna element. It has demonstrated a coupling of −22 dB with ripple of ± 1.5 dB and a limited match at coupled port. This is mainly due to the internal termination of the isolated port and the variation of the load at the through port. Even though the frequency flatness is limited, this is not of concern as it is used for calibration, whereas flatness across the channels is rather important.

The performance of element in array environment is analysed using scan reflection coefficient of an infinite array. The mutual couplings between elements are exploited to get a more beamwidth in array environment and hence scan coverage. This performance of the array is evaluated by measuring the average active element gain pattern. Measured active reflection coefficient of the central element of the 16-element *H*-plane linear phased array is calculated from measured mutual coupling coefficients for broadside scan. The array radiation patterns at scan angles of 0°, 30° and 60° are presented to demonstrate the wide scan angle capability. No grating lobes are observed for ± 60° scan coverage. It also exhibited a low cross-polarisation. This 1×16 *H*-plane linear array finds application to airborne platforms.

© The Institution of Engineering and Technology 2018

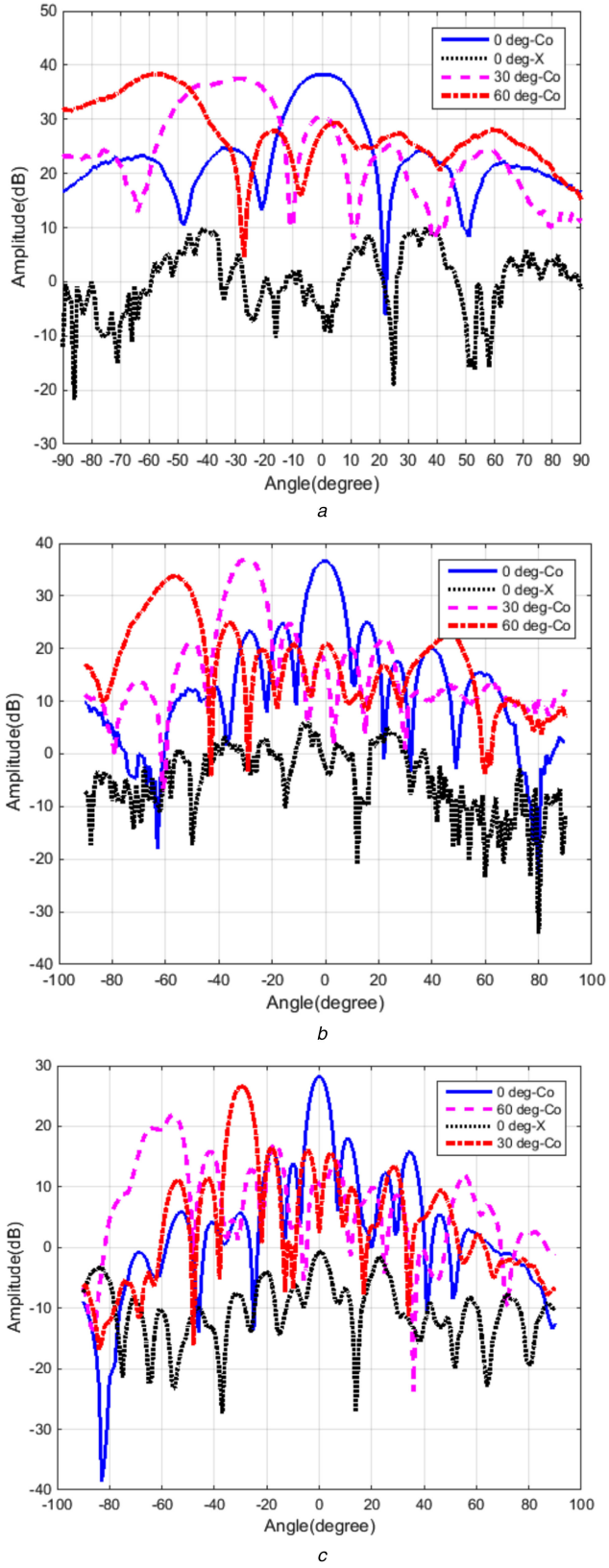

Fig. 9 *Measured array radiation patterns of 16-element linear array*
(a) 6 GHz, ***(b)*** 12 GHz, ***(c)*** 18 GHz at broadside and two scan angles 30° and 60°

7 References

[1] Mailloux, R.J.: '*Phased array handbook*' (Artech House, London, 1994, 2nd edn.2005)

[2] Curtis Schleher, D.: '*Introduction to electronic warfare*' (Artech House, London, 1986)

[3] Bardash, I.: 'Phased arrays for ECM applications', *Microw. J.*, 1982, **25**, pp. 81–92

[4] Lipsky, S.E.: '*Microwave passive direction finding*' (SciTech Publishing, USA, 2004)

[5] Schaubert, D.H., Chio, T.H.: 'Wideband vivaldi arrays for large aperture antennas'. Perspective on Radio Astronomy – Technologies for Large Antenna Arrays, Proc. of Conf. at the ASTRON Institute, April 1999, pp. 49–57

[6] Balanis, C.A.: '*Modern antenna handbook*' (John Wiley& Sons, USA, 2011)

[7] Yihong, F.L., Jiao, Y.C.: 'A 0.7–20GHz strip-fed bilateral tapered slot antenna with low cross polarization', *IEEE Antennas Wirel. Propag. Lett.*, 2013, **12**, pp. 737–740

[8] Skolnik, M.: '*Radar handbook*' (McGraw Hill, USA, 2008, 3rd edn.)

[9] Lee, K., Chu, R., Liu, S.: 'A built-in performance-monitoring/fault isolation and correction (PM/FIC) system for active phased array antennas', *IEEE Trans. Antennas Propag.*, 1993, **41**, (11), pp. 1530–1539

[10] Locke, L., Kordiboroujeni, Z., Bornemann, J., *et al.*: 'Substrate integrated waveguide couplers for tapered slot antennas in adaptive receiver applications'. 7th European Conf. on Antennas and Propagation (EUCAP 2013) - Convened sessions, 2013, pp. 2865–2869

[11] Nikolaou, S., Ponchak, G.E., Papapolymerou, J., *et al.*: 'Conformal double exponentially tapered slot antenna (DETSA) on LCP for UWB applications', *IEEE Trans. Antennas Propag.*, 2006, **54**, (6), pp. 1663–1669

[12] Yngvesson, K.S., Koorzeniowski, T.l., Kim, Y.S., *et al.*: 'The tapered slot antenna-A new integrated element for millimeter-wave applications', *IEEE Trans. Microwave Theory and Techniques*, 1989, **37**, (2), pp. 737–740

[13] Lee, R.Q., Simons, R.N.: 'Effect of curvature on tapered slot antennas'. IEEE antenna and propagation society int. symp., July 1996

[14] Lee, K.F., Chen, W.: '*Advances in microstrip and printed Antennas*' (John Wiley & Sons, NewYork, USA, 1997)

[15] Tu, W., Kim, S., Chang, K.: 'Wideband microstrip-fed tapered slot antennas and phased array', *Int. J. RF Microw. Comput. Aided Eng.*, 2007, pp. 233–242

[16] Revankar, U.K., Priya, S.N., Shukla, S.: 'Linear tapered slot antenna element for broadband wide scan angle active phased array'. Int. Symp. on microwaves, Bangalore, 19–22 December 2008

[17] Lewis, L.R., Fesset, M., Hunt, J.: 'A broadband stripline array element'. IEEE Symp. Antennas and Propagation, Atlanta, USA, June 1974, pp. 335–337

[18] Wang, P., Zhang, H., Wen, G., *et al.*: 'Design of modified 6–18GHz balanced antipodal vivaldi antenna', *Prog. Electromagn. Res. C*, 2012, **25**, pp. 271–285

[19] Langley, J.D.S., Hall, P.S., Newham, P.: 'Balanced antipodal vivaldi antenna for wide bandwidth phased arrays', *IEE Proc. Microw. Antennas Propag.'*, 1996, **143**, (2), pp. 97–102

[20] Kota, K., Shafai, L.: 'Gain and radiation pattern enhancement of balanced antipodal vivaldi antenna', *Electron. Lett.*, 2011, **47**, (5), pp. 303–304

[21] CST Microwave Studio, version 10, CST, Germany

[22] Shin, D.H., Schaubert, D.H.: 'A parametric study of stripline-fed vivaldi notch-antenna arrays', *IEEE Trans. Antennas and Propagation*, 1999, **47**, (5), pp. 879–886

[23] Mongia, R.K., Bahl, I.J., Bhartia, P.: '*RF and microwave coupled-line circuits*' (Artech House, Boston, 2007, 2nd edn.)

[24] Gruszezynski, S., Wineza, K.: 'Broadband multisection asymmetric 8.34-dB directional coupler with improved directivity'. Proc. of Asia-Pacific Microwave Conf., Bangkok, Thailand, 2007

[25] Pozar, D.M.: '*Microwave engineering*' (John Wiley & Sons, USA, 2012, 4th edn.)

[26] Levy, R.: 'Tables for asymmetric multi-element coupled- transmission-line directional couplers', *IEEE Trans. Microwave Theory and Techniques*, 1964, **12**, pp. 275–279

[27] 'OhmegaPly Substrate' http://www.pcbcic.com/docs/Ohmega_Design_Version_18_1.pdf

[28] Bahl, I.J.: '*Lumped elements for RF and microwave circuits*' (Artech House, Boston, 2003)

[29] Hansen, R.C.: '*Phased array antennas*' (John Wiley& Sons, New Jersey, 2009, 2nd edn.)

[30] Holter, H., Steyskal, H.: 'On the size requirement of finite phased-array model', *IEEE Trans. Antennas Propag.*, 2002, **50**, (6), pp. 836–840

[31] Visser, H.J.: '*Array and phased array antenna basics*' (John Wiley& Sons, USA, 2005)

[32] Haupt, R.L.: '*Antenna arrays-A computational approach*' (John Wiley& Sons, USA, 2010)

[33] Kedar, A., Beenamole, K.S.: 'Wide beam tapered slot antenna for wide angle scanning phased array antenna', *Progress in Electromagnetic Research B*, 2011, **27**, pp. 235–252

© The Institution of Engineering and Technology 2018